EUROPEAN ORGANIZATION FOR NUCLEAR RESEARCH

L3 Note 2558
June 28, 2000

Search for anomalous couplings in the Higgs sector at LEP

The L3 Collaboration

Abstract

We search for a Higgs particle with anomalous couplings in the $e^+e^- \to H\gamma$, $e^+e^- \to HZ$ and $e^+e^- \to He^+e^-$ processes with the L3 detector at LEP. We explore the mass range 70 GeV $< m_H <$ 170 GeV using 177 pb^{-1} of integrated luminosity at a center-of-mass energy of $\sqrt{s} = 189$ GeV. The Higgs decays $H \to b\bar{b}$, $H \to \gamma\gamma$ and $H \to Z\gamma$ are considered in the analysis. No evidence for anomalous Higgs production is found. This is interpreted in terms of limits on the anomalous couplings d and d_B, Δg_1^Z and $\Delta\kappa_\gamma$. Limits on the $\Gamma(H \to \gamma\gamma)$ and $\Gamma(H \to Z\gamma)$ partial widths in the explored Higgs mass range are also obtained.

Submitted to the *XXXth International Conference on High Energy Physics*
July 27 - August 2, 2000, Osaka, Japan

1 Introduction

The spontaneous symmetry breaking mechanism is a fundamental ingredient of the Standard Model (SM) [1] of electroweak interactions. Despite its relevance, the experimental information on the Higgs sector of the SM is scarce and indirect at present. The search for the Higgs particle is a key issue for present and future high-energy colliders, and any deviation from expectations could be a clear guide for new physics scenarios beyond the SM.

The SM can be extended via a linear representation of the $SU(2)_L \times U(1)_Y$ symmetry breaking mechanism [2]. The lowest order representation leads to the Standard Model. At higher orders new interactions between the Higgs particle and gauge bosons become possible. They modify the production mechanisms and decay properties of the Higgs. The relevant CP-invariant Lagrangian terms for neutral bosons are the following [3]:

$$\begin{aligned}\mathcal{L}_{\text{eff}} = g_{\mathrm{H}\gamma\gamma}\ \mathrm{HA}_{\mu\nu}\mathrm{A}^{\mu\nu} \ +\ g^{(1)}_{\mathrm{HZ}\gamma}\ \mathrm{A}_{\mu\nu}\mathrm{Z}^{\mu}\partial^{\nu}\mathrm{H} \ +\ g^{(2)}_{\mathrm{HZ}\gamma}\ \mathrm{HA}_{\mu\nu}\mathrm{Z}^{\mu\nu} \\ +\ g^{(1)}_{\mathrm{HZZ}}\ \mathrm{Z}_{\mu\nu}\mathrm{Z}^{\mu}\partial^{\nu}\mathrm{H} \ +\ g^{(2)}_{\mathrm{HZZ}}\ \mathrm{HZ}_{\mu\nu}\mathrm{Z}^{\mu\nu} \ +\ g^{(3)}_{\mathrm{HZZ}}\ \mathrm{HZ}_{\mu}\mathrm{Z}^{\mu}\end{aligned} \tag{1}$$

where A_μ, Z_μ and H are the photon, Z and Higgs fields, respectively, and $\mathrm{X}_{\mu\nu} = \partial_\mu \mathrm{X}_\nu - \partial_\nu \mathrm{X}_\mu$. The couplings $g_{\mathrm{H}\gamma\gamma}$, $g^{(1)}_{\mathrm{HZ}\gamma}$, $g^{(2)}_{\mathrm{HZ}\gamma}$, $g^{(1)}_{\mathrm{HZZ}}$, $g^{(2)}_{\mathrm{HZZ}}$ and $g^{(3)}_{\mathrm{HZZ}}$ can be parametrized as follows [4–6]:

$$g_{\mathrm{H}\gamma\gamma} = \frac{g}{2m_{\mathrm{W}}}\ \left(d\sin^2\theta_{\mathrm{W}} + d_B\cos^2\theta_{\mathrm{W}}\right) \tag{2}$$

$$g^{(1)}_{\mathrm{HZ}\gamma} = \frac{g}{m_{\mathrm{W}}}\ \left(\Delta g_1^{\mathrm{Z}}\sin 2\theta_{\mathrm{W}} - \Delta\kappa_\gamma\tan\theta_{\mathrm{W}}\right) \tag{3}$$

$$g^{(2)}_{\mathrm{HZ}\gamma} = \frac{g}{2m_{\mathrm{W}}}\ \sin 2\theta_{\mathrm{W}}\ \ (d - d_B) \tag{4}$$

$$g^{(1)}_{\mathrm{HZZ}} = \frac{g}{m_{\mathrm{W}}}\ \left(\Delta g_1^{\mathrm{Z}}\cos 2\theta_{\mathrm{W}} + \Delta\kappa_\gamma\tan^2\theta_{\mathrm{W}}\right) \tag{5}$$

$$g^{(2)}_{\mathrm{HZZ}} = \frac{g}{2m_{\mathrm{W}}}\ \left(d\cos^2\theta_{\mathrm{W}} + d_B\sin^2\theta_{\mathrm{W}}\right) \tag{6}$$

$$g^{(3)}_{\mathrm{HZZ}} = \frac{g\ m_{\mathrm{W}}}{2}\delta_{\mathrm{Z}} \tag{7}$$

where g is the $\mathrm{SU(2)_L}$ coupling constant, θ_{W} is the Weinberg angle and m_{W} is the W mass. The five anomalous couplings d, d_B, Δg_1^{Z}, $\Delta\kappa_\gamma$ and δ_{Z} constitute a convenient set of adimensional parameters to describe deviations in Higgs-vector boson interactions. They are not severely constrained by electroweak measurements at the Z pole or low energies [3, 7]. The couplings d and d_B have been introduced in [4], while the couplings Δg_1^{Z} and $\Delta\kappa_\gamma$ are commonly used in the context of $\mathrm{e^+e^-} \to \mathrm{W^+W^-}$ studies [5]. Limits on the parameter $\xi = (1 + \delta_{\mathrm{Z}})$, which quantifies deviations in the magnitude of HZZ, HWW couplings [6] have already been set in Reference [8] and will not be further discussed in this paper.

A typical anomalous signature would be the observation of large $\mathrm{H} \to \gamma\gamma$ and $\mathrm{H} \to \mathrm{Z}\gamma$ branching fractions, which are zero in the SM at tree level. In addition, a search for anomalous Higgs production with non-zero Δg_1^{Z} or $\Delta\kappa_\gamma$ couplings offers a complementary way to look for the same type of deviations studied in the $\mathrm{e^+e^-} \to \mathrm{W^+W^-}$ process.

The data used in this analysis have been collected with the L3 detector [9] at a center-of-mass energy of $\sqrt{s} = 189$ GeV and correspond to an integrated luminosity of 177 pb^{-1}. Previous experimental analyses on anomalous Higgs production accompanied by photons can be found in [10].

2 Analysis strategy and Monte Carlo samples

We search for a Higgs particle emitted in the $e^+e^- \to H\gamma$ and $e^+e^- \to He^+e^-$ processes at a center-of-mass energy of $\sqrt{s} = 189$ GeV. These processes are enhanced by the presence of anomalous $H\gamma\gamma$ and $HZ\gamma$ couplings and have sensitivity to Higgs masses up to the center-of-mass energy of the collision: $m_H < \sqrt{s}$. The analysis is complemented with the results from L3 $e^+e^- \to HZ$ searches [11, 12], which are sensitive to anomalous HZZ and $HZ\gamma$ couplings for Higgs masses below the kinematic limit: $m_H < \sqrt{s} - m_Z$. All three anomalous possibilities are shown in Figure 1.

In order to search for the anomalous $e^+e^- \to H\gamma$ process (Figure 1a) a dedicated generator is written. It assumes the expected $(1 + \cos^2\theta_H)\ d(cos\theta_H)$ dependence for the differential cross section as a function of the Higgs production angle, θ_H. The generator is interfaced with the L3 simulation and reconstruction programs and takes into account initial state radiation [13] and photon emission by final-state particles [14]. The generator takes also into account spin correlations and off-shell contributions in cascade decays like $H \to Z\gamma \to f\bar{f}\gamma$.

The $e^+e^- \to He^+e^-$ process (Figure 1b) is interpreted as the production of a narrow-width spin-zero resonance (the Higgs particle) in two-photon processes. For the generation of this process the PC generator [15] is used. Finally, the standard $e^+e^- \to HZ$ search channel is also affected by the presence of anomalous couplings (Figure 1c). The expression for the differential cross section in this case can be found in Reference [16].

For the determination of the branching fractions and partial widths of an anomalous Higgs, References [17] and [18] are used. The search is restricted to the Higgs mass range 70 GeV $< m_H <$ 170 GeV. The decay channels $H \to \gamma\gamma$, $H \to Z\gamma$ and $H \to b\bar{b}$ are considered. The cases $H \to \gamma\gamma$ and $H \to Z\gamma$ complement each other in sensitivity, probing a large part of the parameter space. The $H \to b\bar{b}$ decay is dominant in the particular region where $H \to \gamma\gamma$ is strongly suppressed and $H \to Z\gamma$ is kinematically forbidden ($m_H \lesssim m_Z$).

The analysis is performed as a function of the Higgs mass. Signal events are generated for the following six Higgs masses: 70, 90, 110, 130, 150 and 170 GeV. For each mass under consideration and for each process under study more than 2000 signal events are generated. For the analysis of the $e^+e^- \to HZ$ process, we reinterpret the cross section limits obtained by L3 from SM [11] and fermiophobic [12] Higgs searches.

For the study of SM backgrounds the following generators are considered: KK2F [19] and PYTHIA [20] for $e^+e^- \to q\bar{q}(\gamma)$ contaminations, PYTHIA for multiperipheral $e^+e^- \to e^+e^-q\bar{q}$ events, GGG [21] for $e^+e^- \to \gamma\gamma(\gamma)$ events, KORALW [22] for $e^+e^- \to W^+W^-$, EXCALIBUR [23] for $e^+e^- \to We\nu$ and remaining four-fermion backgrounds at high invariant masses, and KORALZ [24] for $e^+e^- \to \tau^+\tau^-(\gamma)$ events. In all cases the Monte Carlo (MC) statistics used in the analysis is more than 10 times the statistics present in data, except for multiperipheral $e^+e^- \to e^+e^-q\bar{q}$ events, for which the relative factor is 2.

All MC samples are generated, simulated in the L3 detector and reconstructed in the same way as data. Detector inefficiencies as a function of time are taken into account.

3 Event selection

The $e^+e^- \to H\gamma$ and $e^+e^- \to He^+e^-$ Higgs production mechanisms lead to characteristic topologies. In an $e^+e^- \to H\gamma$ process a high-energy photon of fixed energy is produced, and typically most of the collision energy is visible in the final state. Events originating from a two-photon collision, $e^+e^- \to He^+e^-$, have missing longitudinal momentum and missing mass, as

the two emerging electrons tend to escape detection at very low polar angles. The analysis of the specific channel $e^+e^- \to H\gamma, H \to Z\gamma$, is based on the $e^+e^- \to Z\gamma\gamma$ selection criteria described in Reference [25]. The analysis is performed in Higgs mass steps of 1 GeV by interpolation of the generated Higgs signal efficiencies. This is particularly relevant in the case of photonic Higgs decays, where the good energy resolution of the L3 detector can be exploited efficiently.

A basic ingredient in the study is photon identification. In all analyses except for $e^+e^- \to H\gamma, H \to Z\gamma$, a photon candidate is defined as a shower in the electromagnetic calorimeter with a profile consistent with that of a photon (more than 90% of its energy contained in a 3×3 crystal matrix) and with no associated track in the vertex chamber. In addition, all photon candidates must satisfy $E_\gamma > 5$ GeV and $|\cos\theta_\gamma| < 0.8$, where E_γ is the photon energy and θ_γ is its polar angle. These cuts reduce the background associated to initial and final-state radiation, while keeping a large efficiency for the Higgs signal.

A second ingredient is the identification of $H \to b\bar{b}$ decays. The b-tagging performance is similar to the one obtained in the L3 SM Higgs search [26].

The statistical treatment is common to all selections. Data samples are assumed to follow a Poisson distribution, according to the expected background and the signal hypothesis under consideration. All quoted limits are determined following a Bayesian approach and assuming a flat prior distribution for the signal cross section.

3.1 $e^+e^- \to H\gamma \to \gamma\gamma\gamma$ analysis

In order to select $e^+e^- \to H\gamma \to \gamma\gamma\gamma$ events we require three photon candidates in the event with a total electromagnetic energy larger than $\sqrt{s}/2$. In addition, the invariant mass of (at least) one of the photon pairs in the event, $M_{\gamma\gamma}$, must be consistent with the Higgs mass hypothesis: $|M_{\gamma\gamma} - m_H| < 3$ GeV.

After these cuts the contamination from processes other than $e^+e^- \to \gamma\gamma(\gamma)$, as estimated from MC simulations, is found to be negligible. In Figure 2a the distribution of the invariant mass in data and in MC for one of the Higgs mass hypotheses with largest signal significance ($m_H = 156$ GeV) is shown.

The number of expected and observed events, the signal efficiency in the full phase space, and the limit on $\sigma(e^+e^- \to H\gamma)\ \mathrm{Br}(H \to \gamma\gamma)$ at the 95% confidence level (CL) are shown in Table 1 for several Higgs mass hypotheses. No evidence for any anomalous signal is observed, leading to the limits shown in Figure 3.

m_H (GeV)	Data events	Background events	Signal acceptance (%)	95% CL Upper Limit on $\sigma(e^+e^- \to H\gamma)\ \mathrm{Br}(H \to \gamma\gamma)$ (fb)
70	0	1.26	22.2	70
90	1	0.83	20.8	115
110	1	0.83	19.7	122
130	0	0.75	18.9	91
150	0	0.91	18.5	93
170	2	1.89	18.4	152

Table 1: Number of selected candidates, background events, signal acceptance and 95% CL cross section limits after the $e^+e^- \to H\gamma \to \gamma\gamma\gamma$ selection for different Higgs mass hypotheses.

3.2 $e^+e^- \to H\gamma \to b\bar{b}\gamma$ analysis

High particle multiplicity and momentum balance cuts are applied in order to select an initial sample of hadronic events. A $b\bar{b}\gamma$ event is finally tagged by the presence of an isolated photon (its energy must account for more than 90% of the jet energy) and of B-hadrons (the event tag discriminant, $\mathcal{D}$, must satisfy $\mathcal{D} > 1.5$).

Most of the contamination in the selected sample is due to the almost irreducible SM process: $e^+e^- \to Z\gamma$. The remaining backgrounds from Weν, $q\bar{q}e^+e^-$ and misidentified photons in $q\bar{q}$ are estimated to be at the 1% level.

The distribution of the recoiling mass to the photon in data and in MC for one of Higgs mass hypotheses with largest signal significance ($m_H = 140$ GeV) are shown in Figure 2b. These distributions are used to set limits at 95 % CL on the $\sigma(e^+e^- \to H\gamma)$ Br$(H \to b\bar{b})$ magnitude. We find that the data are consistent with MC in the absence of a Higgs signal, leading to the limits shown in Figure 3.

m_H (GeV)	Data events	Background events	Signal acceptance (%)	95% CL Upper Limit on $\sigma(e^+e^- \to H\gamma)$ Br$(H \to b\bar{b})$ (fb)
70	2	2.8	20.8	101
90	77	83.7	24.7	365
110	21	20.7	22.5	200
130	9	10.7	20.2	155
150	3	10.3	18.8	105
170	10	16.0	17.6	157

Table 2: Number of selected candidates, background events, signal acceptances and cross section limits after the $e^+e^- \to H\gamma \to b\bar{b}\gamma$ selection for different Higgs mass hypotheses.

3.3 $e^+e^- \to H\gamma \to Z\gamma\gamma$ analysis

The selection criteria for this channel are described in Reference [25]. We select 36 events, in agreement with the expected SM background of 39.2.

The signal efficiency over the full phase space and the 95% CL limits on $\sigma(e^+e^- \to H\gamma)$ Br$(H \to Z\gamma)$ are shown in Table 3 for different Higgs masses. The signal efficiency is interpolated and the analysis is repeated in mass steps of 1 GeV, leading to the limits shown in Figure 3.

m_H (GeV)	Signal acceptance (%)	95% CL Upper Limit on $\sigma(e^+e^- \to H\gamma)$ Br$(H \to Z\gamma)$ (fb)
95	9.3	723
100	28.6	234
110	33.5	200
130	36.0	186
150	34.5	194
170	34.2	196

Table 3: Signal acceptances and cross section limits after the $e^+e^- \to H\gamma \to Z\gamma\gamma$ selection for different Higgs mass hypotheses.

3.4 $e^+e^- \to He^+e^-$, $H \to \gamma\gamma$ analysis

The selection of the $e^+e^- \to He^+e^-$, $H \to \gamma\gamma$ signal requires the presence of two photon candidates in the event. In addition, a kinematic fit to the signal hypothesis is performed. We assume that all the energy-momentum is lost in the beam pipe and that the visible mass of the event is consistent with m_H within the experimental uncertainties. Finally the χ^2 of the fit is required to be less than $50 - 0.2\ m_H$, where m_H is expressed in GeV.

The distribution of the two photon invariant mass for data and MC after the kinematic fit are shown in Figure 2c for one of the Higgs mass hypotheses with largest signal significance. The background is dominated by $e^+e^- \to \gamma\gamma(\gamma)$ events. Since $\sigma(e^+e^- \to He^+e^-)$ is proportional to the partial Higgs width into photons, $\Gamma(H \to \gamma\gamma)$, the limits to the cross section of the process are directly interpreted in terms of $\Gamma(H \to \gamma\gamma)$ Br$(H \to \gamma\gamma)$. The number of expected and observed events, the signal efficiency over the full phase space and the 95% CL limit on $\Gamma(H \to \gamma\gamma)$ Br$(H \to \gamma\gamma)$ are shown in Table 4 for several Higgs mass hypotheses. There is no evidence for any anomalous signal, leading to the limits shown in Figure 4.

m_H (GeV)	Data events	Background events	Signal acceptance (%)	95% CL Upper Limit on $\Gamma(H \to \gamma\gamma)$ Br$(H \to \gamma\gamma)$ (MeV)
70	0	0.0	22.9	0.3
90	0	1.1	27.5	0.8
110	4	2.6	31.4	4.5
130	6	4.8	34.7	11.6
150	10	9.9	37.3	32.7
170	19	28.7	39.2	88.7

Table 4: Number of selected candidates, background events, signal acceptances and limits on $\Gamma(H \to \gamma\gamma)$ Br$(H \to \gamma\gamma)$ from the $e^+e^- \to e^+e^-H \to e^+e^-\gamma\gamma$ selection for different Higgs mass hypotheses.

3.5 $e^+e^- \to He^+e^-$, $H \to b\bar{b}$ analysis

Similarly to the $e^+e^- \to b\bar{b}\gamma$ case, high particle multiplicity and transverse momentum balance cuts are applied in order to select an initial sample of hadronic events. Since we expect large missing momenta in the case of $e^+e^- \to He^+e^-$ events, no longitudinal momentum cuts are applied. Most of the two-photon events are rejected by requiring a visible event mass greater than 50 GeV, and the b-quark purity is increased by a cut on the the event tag discriminant ($\mathcal{D} > 2$). As for the $e^+e^- \to e^+e^-H \to e^+e^-\gamma\gamma$ case, a kinematic fit is performed, in which only events with two jets (a Durham algorithm with $y_{cut} = 0.05$ is used) are kept. Only events with a good χ^2 fit to the Higgs signal hypothesis $\chi^2_{fit} < 25$ are selected. Finally, a cut on missing mass after kinematic fit is applied in order to reject a large fraction of the $e^+e^- \to b\bar{b}\gamma$ background. For large Higgs masses ($m_H > 95$ GeV), we require $M_{miss} > 0.09\sqrt{s}$. For Higgs masses below or at the Z mass, there is a tighter requirement: $M_{miss} > 0.44\sqrt{s}$. Figure 2d shows the invariant mass distribution of the event after kinematic fit for the Higgs mass hypothesis $m_H = m_Z$. The Z background is largely suppressed due to the stringent cut on the longitudinal invariant mass.

After these cuts, the remaining background corresponds mostly to $e^+e^- \to q\bar{q}(\gamma)$ events, with a small contribution from $e^+e^- \to W^+W^-$ and non-resonant $e^+e^- \to e^+e^-q\bar{q}$ events. The χ^2 distributions of the kinematic fit show the largest sensitivity and are used to set limits on

$\Gamma(H \to \gamma\gamma)$ Br$(H \to b\bar{b})$. We find that the data are consistent with MC in the absence of a Higgs signal, leading to the limits shown in Figure 4.

m_H (GeV)	Data events	Background events	Signal acceptance (%)	95% CL Upper Limit on $\Gamma(H \to \gamma\gamma)$ Br$(H \to b\bar{b})$ (MeV)
70	188	182.3	15.4	2.7
90	107	112.9	16.5	6.6
110	222	232.6	28.7	19.7
130	298	323.9	28.3	43.1
150	388	399.6	29.9	90.9
170	367	369.3	28.4	462.7

Table 5: Number of selected candidates, background events, signal acceptances and limits on $\Gamma(H \to \gamma\gamma)$ Br$(H \to b\bar{b})$ from the $e^+e^- \to e^+e^-H \to e^+e^-b\bar{b}$ selection for different Higgs mass hypotheses.

4 Limits on anomalous couplings

The analysis performed over the different Higgs production mechanism and decay channels samples show that experimental data agrees with SM MC predictions, thus leaving no room for a possible anomalous Higgs signal in the mass range under study. For this reason, the strategy followed is to constrain the possible values allowed for the anomalous couplings at 95% CL.

4.1 One-dimensional limits

In this section exclusion limits for each individual coupling are set as a function of the Higgs mass. The exclusion limits are determined following similar criteria to the ones employed in the standard Higgs search [8]. For a given coupling Δ, a point in the (m_H, Δ) plane is considered as excluded at the 95% CL if the ratio of the confidence level for the signal+background hypothesis to the confidence level for the background-only hypothesis is less than 0.05. All couplings except for Δ are assumed to be zero.

The results for the four anomalous couplings: d, d_B, Δg_1^Z and $\Delta\kappa_\gamma$ are shown in Figures 5 and 6. In addition to the combined result obtained using all processes under study, the individual results for the most sensitive channels are also shown.

In all cases, the $e^+e^- \to HZ$ searches are enough to exclude the region $m_H \lesssim \sqrt{s} - m_Z$ for any value of the anomalous coupling. The fermiophobic $e^+e^- \to HZ, H \to \gamma\gamma$ search is sensitive at large values of d and d_B, for which there is an enhancement of the $H \to \gamma\gamma$ branching fraction. The standard search: $e^+e^- \to HZ, H \to b\bar{b}$ or $\tau^+\tau^-$ covers the region $d \approx d_B \approx 0$.

The $e^+e^- \to H\gamma \to \gamma\gamma\gamma$ and $e^+e^- \to e^+e^-H \to e^+e^-\gamma\gamma$ channels are specially sensitive if the $H\gamma\gamma$ coupling is large, i.e. when the combination $d\sin^2\theta_W + d_B\cos^2\theta_W$ is sizeable (Figure 5). On the contrary, the $e^+e^- \to H\gamma \to Z\gamma\gamma$ process has a dominant role when $H \to \gamma\gamma$ is suppressed (Figure 6). This is the case of the fits to Δg_1^Z and $\Delta\kappa_\gamma$ in the interesting Higgs mass range $m_Z < \sqrt{s} < 2m_W$. The sensitivity of the $e^+e^- \to H\gamma \to b\bar{b}\gamma$ channel (figure 6 at $m_H \approx m_Z$) concerns the region in which $H \to \gamma\gamma$ is small, the $HZ\gamma$ coupling is large and the $H \to Z\gamma$ decay is kinematically not possible. The sensitivity of the $e^+e^- \to e^+e^-H \to e^+e^-b\bar{b}$

process is not large. This is due to the difficulty to get large $H \to b\bar{b}$ branching fractions when a large $H\gamma\gamma$ coupling is required.

The sensitivity of the analysis degrades rapidly when m_H approaches the $2m_W$ threshold, where the $H \to W^+W^-$ becomes dominant even in the presence of relatively large anomalous couplings.

Another usual assumption [3] is to consider that all anomalous interactions have the same strengths at the scale of new physics: $\Delta\kappa_\gamma = -d = -d_B/\tan^2\theta_W = 2\cos^2\theta_W\ \Delta g_1^Z$. Such a choice [1)], although reasonable in what concerns orders of magnitude, is very particular, since it implies the absence of an anomalous $H \to Z\gamma$ decay and a large exclusion power for the channels sensitive to the $H\gamma\gamma$ coupling. We show the excluded regions under this assumption in Figures 5-6.

4.2 Two-dimensional limits

The 95% CL contours obtained from a likelihood fit in the (d, d_B) plane, taking into account all analyzed processes, are shown in Figure 7 for different Higgs masses. In the fit we assume that the couplings Δg_1^Z, $\Delta\kappa_\gamma$ are zero. The $e^+e^- \to H\gamma \to Z\gamma\gamma$ process helps in excluding large values of the anomalous couplings in the region where $d\sin^2\theta_W + d_B\cos^2\theta_W \approx 0$. The fit is reinterpreted as a fit in the $(\Gamma(H \to \gamma\gamma), \Gamma(H \to Z\gamma))$ plane. The results are also presented in Figure 7 for different Higgs masses.

In summary, Higgs masses below the kinematic limit $m_H < \sqrt{s} - m_Z$ are found to be inconsistent with the data even in the presence of anomalous couplings. Their possible existence for Higgs masses below the threshold of $H \to W^+W^-$ production is highly constrained. Upper limits to the $\Gamma(H \to \gamma\gamma)$ and $\Gamma(H \to Z\gamma)$ partial widths in the region of interest for present and future colliders are also obtained.

Acknowledgments

We wish to express our gratitude to the CERN accelerator divisions for the excellent performance of the LEP machine. We acknowledge the contributions of the engineers and technicians who have participated in the construction and maintenance of this experiment.

References

[1] S.L. Glashow, Nucl. Phys. **22** (1961) 579;
S. Weinberg, Phys. Rev. Lett. **19** (1967) 1264;
A. Salam, "Elementary Particle Theory", Ed. N. Svartholm, Stockholm, Almqvist and Wiksell (1968), 367;
P.W. Higgs, Phys. Lett. **12** (1964) 132.

[2] W. Buchmüller and D. Wyler, Nucl. Phys. **B 268**, (1986) 621;
C.J.C. Burgess and H.J. Schnitzer, Nucl. Phys. **B 228** (1983) 424;
C.N. Leung, S.T. Love and S. Rao, Z. Phys. **C 31** (1986) 433.

[1)] The previous assumption is equivalent to $m_W^2\ F/\Lambda^2 = \Delta\kappa_\gamma = -d = -d_B/\tan^2\theta_W = 2\cos^2\theta_W\ \Delta g_1^Z$, where Λ is the scale of new physics and F is a constant of order one. Our results are trivially reinterpreted as exclusion regions in the $(F/\Lambda^2, m_H)$ plane.

[3] O.J.P. Éboli *et al.*, Phys. Lett. **B 434** (1998) 340;
M.C. González-García, Int. J. Mod. Phys. **A 14** (1999) 3121.

[4] G.J. Gounaris, F.M. Renard and N.D. Vlachos, Nucl. Phys. **B 459** (1996) 51.

[5] K. Hagiwara *et al.*, Nucl. Phys. **B 282** (1987) 253.

[6] B. Grządkowski and J. Wudka, Phys. Lett. **B 364** (1995) 49.

[7] S. Alam, S. Dawson and R. Szalapski, Phys. Rev. **D 57** (1998) 1577.

[8] The ALEPH, DELPHI, L3 and OPAL Collaborations and the LEP Working Group for Higgs boson Searches, CERN-EP-2000-055 (2000).

[9] B.Adeva *et al.*, L3 Collaboration, Nucl. Inst. Meth. **A289** (1990) 35;
J.A.Bakken *et al.*, Nucl. Inst. Meth. **A275** (1989) 81;
O.Adriani *et al.*, Nucl. Inst. Meth. **A302** (1991) 53;
B.Adeva *et al.*, Nucl. Inst. Meth. **A323** (1992) 109;
K.Deiters *et al.*, Nucl. Inst. Meth. **A323** (1992) 162;
M.Chemarin *et al.*, Nucl. Inst. Meth. **A349** (1994) 345;
G.Basti *et al.*, Nucl. Inst. Meth. **A374** (1996) 293;
A.Adam *et al.*, Nucl. Inst. Meth. **A383** (1996) 342.

[10] DELPHI Collaboration, P. Abreu *et al.*, Phys. Lett. **B 458** (1999) 431.

[11] L3 Collaboration, M. Acciarri *et al.*, Phys. Lett. **B 461** (1999) 376.

[12] L3 Collaboration, M. Acciarri *et al.*, "Search for Higgs Boson Decaying into Two Photons in e^+e^- Interactions at $\sqrt{s} = 189$ GeV", in preparation.

[13] F.A. Berends and R. Kleiss, Nucl. Phys. **B 260** (1985) 32.

[14] E. Barberio and Z. Wąs, Comp. Phys. Comm. **79** (1994) 291.

[15] F.L. Linde, "Charm Production in Two-Photon Collisions", Ph.D. Thesis, Rijksuniversiteit Leiden 1988.

[16] K. Hagiwara and M.L. Stong, Z. Phys. **C 62** (1994) 99.

[17] K. Hagiwara, R. Szalapski and D. Zeppenfeld, Phys. Lett. **B 318** (1993) 155.

[18] J.C. Romao and S. Andringa, Eur. Phys. J. **C7** (1999) 631.

[19] S. Jadach, B.F.L. Ward and Z. Wąs, Preprint CERN-TH/99-235, hep-ph/9912214.

[20] T. Sjöstrand, Comp. Phys. Comm. **82** (1994) 74.

[21] F. A. Berends and R. Kleiss, Nucl. Phys. **B 186** (1981) 22.

[22] M. Skrzypek *et al.*, Comp. Phys. Comm. **94** (1996) 216;
M. Skrzypek *et al.*, Phys. Lett. **B 372** (1996) 289.

[23] F.A. Berends, R. Kleiss and R. Pittau, Nucl. Phys. **B 424** (1994) 308; Nucl. Phys. **B 426** (1994) 344; Nucl. Phys. (Proc. Suppl.) **B 37** (1994) 163;
R. Kleiss and R. Pittau, Comp. Phys. Comm. **83** (1994) 141;
R. Pittau, Phys. Lett. **B 335** (1994) 490.

[24] S. Jadach, B. F. L. Ward and Z. Wąs, Comp. Phys. Comm. **79** (1994) 503.

[25] L3 Collaboration, M. Acciarri *et al.*, Phys. Lett. **B 478** (2000) 39.

[26] L3 Collaboration, M. Acciarri *et al.*, Phys. Lett. **B 411** (1997) 373.

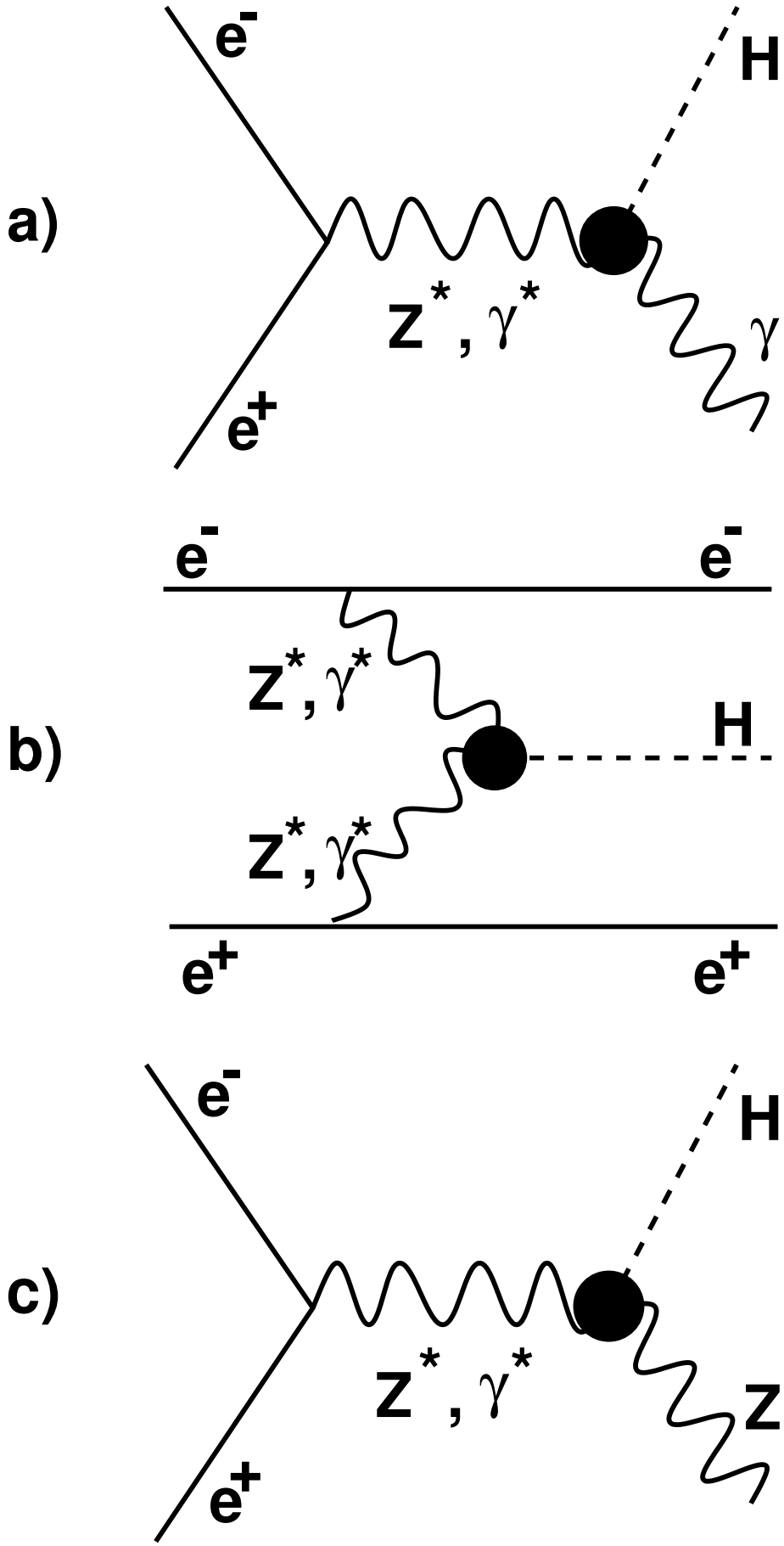

Figure 1: Relevant processes in the search for $H\gamma\gamma$, $HZ\gamma$ and HZZ anomalous couplings at LEP: a) $e^+e^- \to H\gamma$, b) $e^+e^- \to He^+e^-$ and c) $e^+e^- \to HZ$.

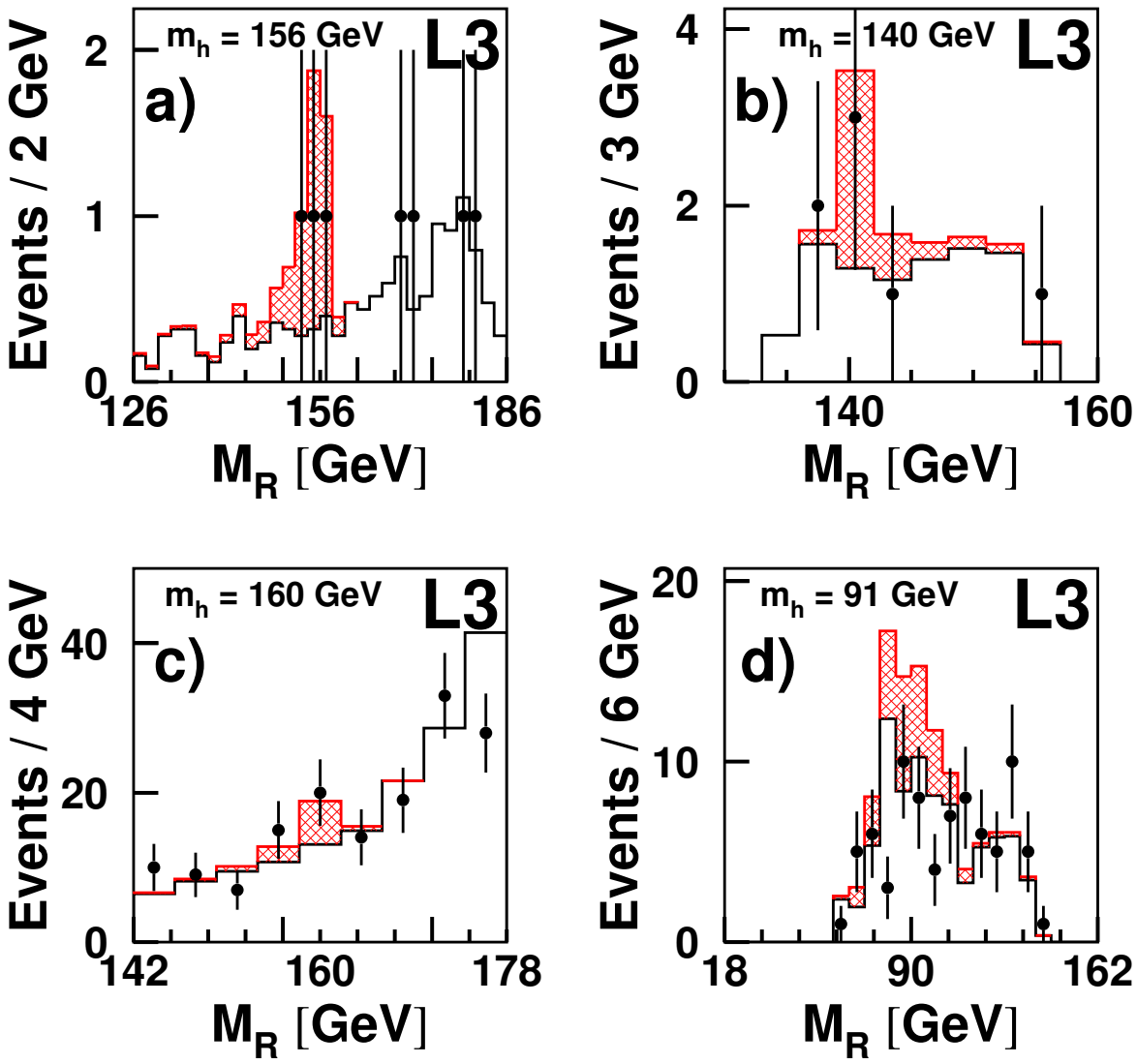

Figure 2: Distributions of the reconstructed Higgs mass, M_R, for a) $e^+e^- \to H\gamma \to \gamma\gamma\gamma$ event candidates at $m_H = 156$ GeV, b) $e^+e^- \to H\gamma \to b\bar{b}\gamma$ candidates at $m_H = 140$ GeV, c) $e^+e^- \to e^+e^-H \to e^+e^-\gamma\gamma$ candidates at $m_H = 160$ GeV, and d) $e^+e^- \to e^+e^-H \to e^+e^-b\bar{b}$ candidates at $m_H = 91$ GeV. In all plots, points are data and the white histogram is the background. For cases a), b) and c) a Higgs signal with a cross section of 0.1 pb is added to the background and superimposed on the plot. The three cases correspond to Higgs mass hypotheses with a relevant signal significance. Case d) illustrates the large suppression of $e^+e^- \to Z\gamma$ background events obtained in the $e^+e^- \to e^+e^-H \to e^+e^-b\bar{b}$ selected sample. The superimposed signal cross section in this case is 1 pb.

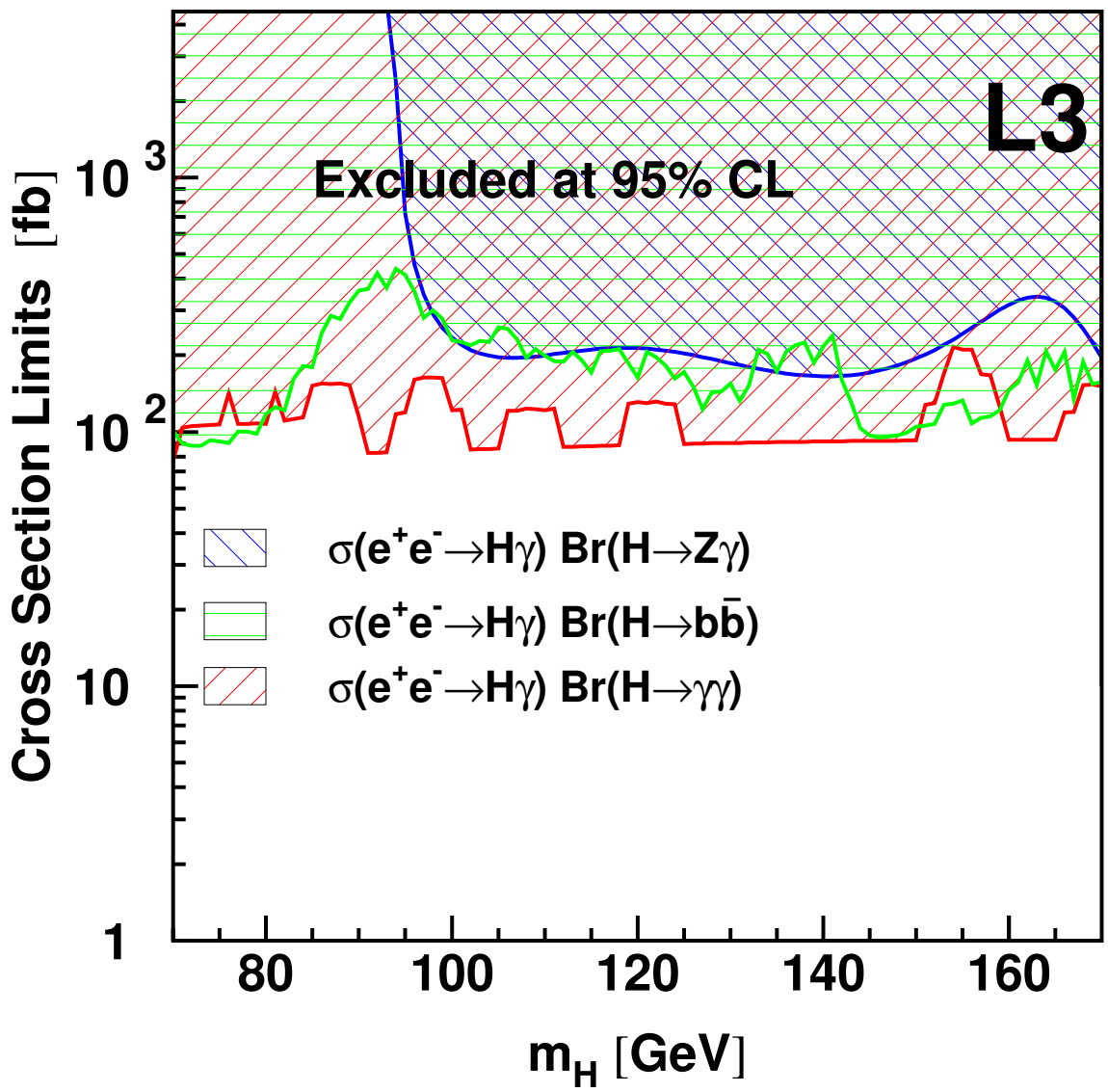

Figure 3: Cross section upper limits as a function of the Higgs mass, m_{H}, for the $\mathrm{e^+e^-} \to \mathrm{H}\gamma \to \gamma\gamma\gamma$, $\mathrm{e^+e^-} \to \mathrm{H}\gamma \to \mathrm{b\bar{b}}\gamma$ and $\mathrm{e^+e^-} \to \mathrm{H}\gamma \to \mathrm{Z}\gamma\gamma$ processes in the presence of anomalous Higgs couplings at $\sqrt{s} = 189$ GeV.

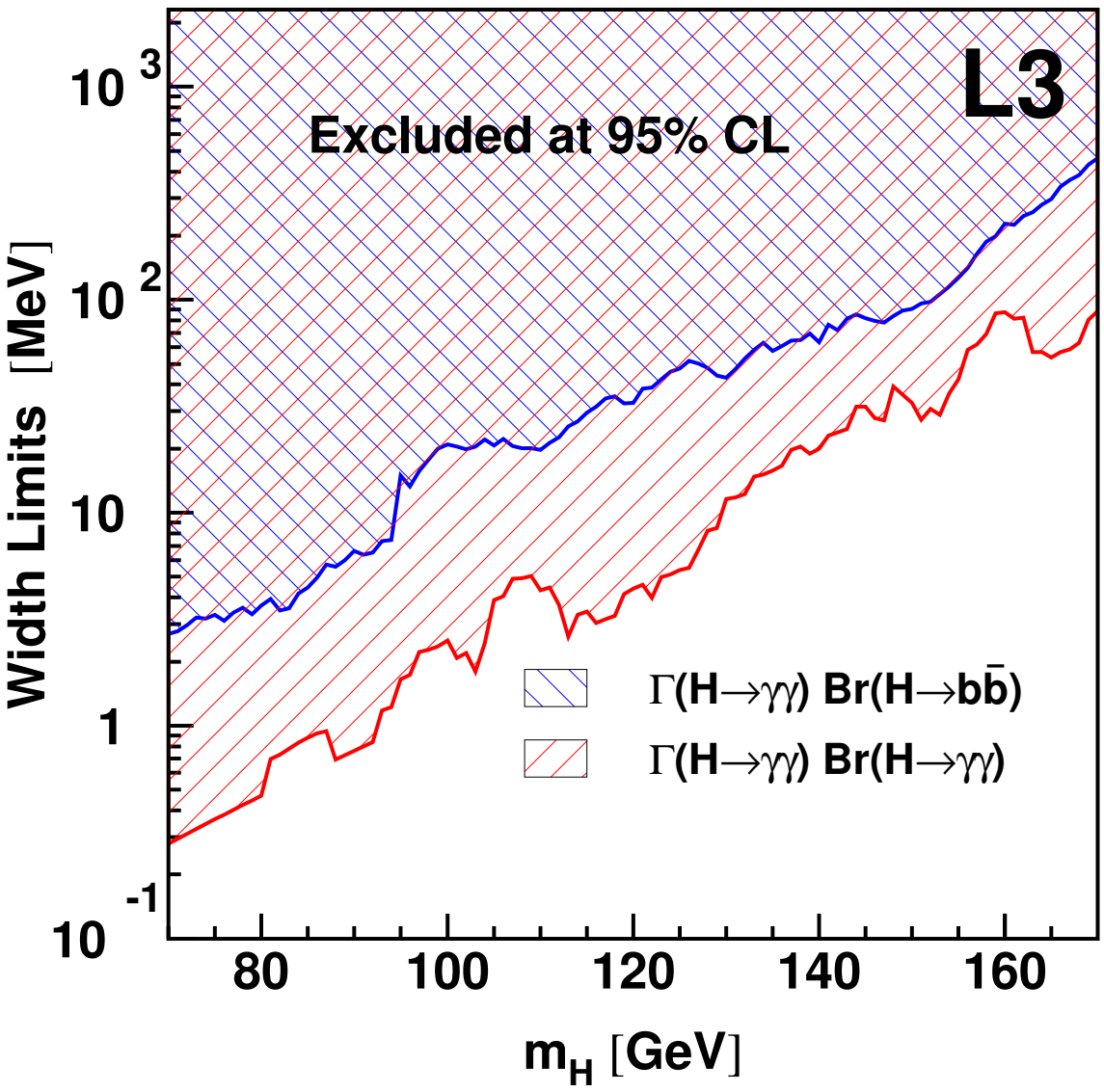

Figure 4: Upper limits of the quantities $\Gamma(\mathrm{H} \to \gamma\gamma)\ \mathrm{Br}(\mathrm{H} \to \gamma\gamma)$ and $\Gamma(\mathrm{H} \to \gamma\gamma)\ \mathrm{Br}(\mathrm{H} \to \mathrm{b\bar{b}})$ as a function of the Higgs mass, m_{H}, from the analysis of the $\mathrm{e^+e^-} \to \mathrm{He^+e^-}$ process in the presence of anomalous Higgs couplings at $\sqrt{s} = 189$ GeV.

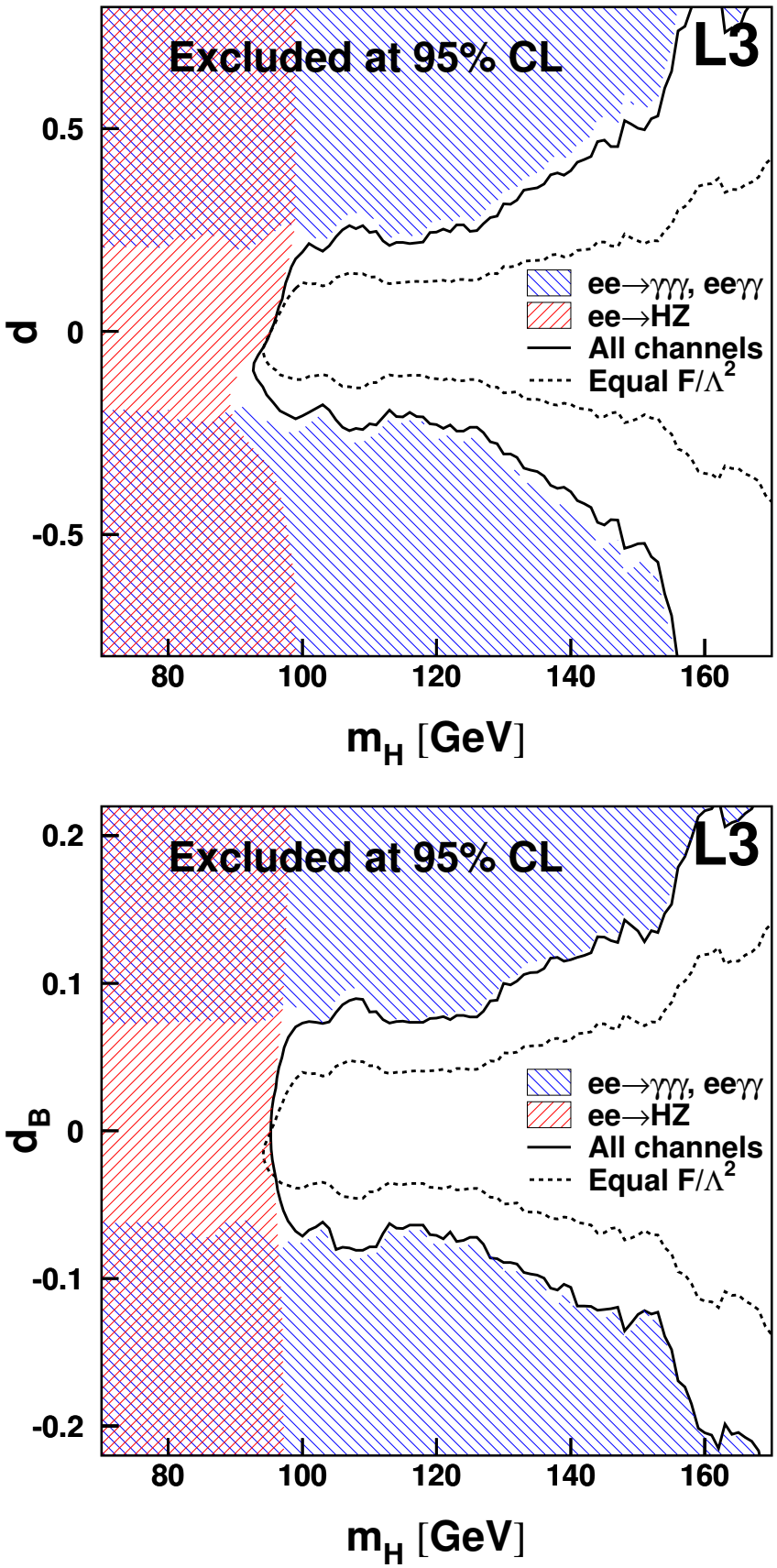

Figure 5: Excluded regions for the anomalous couplings d and d_B as a function of the Higgs mass, m_{H}. Limits on d are obtained under the assumption $d_B = \Delta g_1^{\mathrm{Z}} = \Delta\kappa_\gamma = 0$, while limits on d_B assume the relation $d = \Delta g_1^{\mathrm{Z}} = \Delta\kappa_\gamma = 0$. The regions excluded by the most sensitive analyses: $\mathrm{e^+e^-} \to \mathrm{H}\gamma \to \gamma\gamma\gamma$, $\mathrm{e^+e^-} \to \mathrm{e^+e^-H} \to \mathrm{e^+e^-}\gamma\gamma$ and $\mathrm{e^+e^-} \to \mathrm{HZ}$ are also shown. In addition, we show the limits reached under the assumption of equal couplings at a scale of new physics Λ (dashed lines): $m_{\mathrm{W}}^2\ F/\Lambda^2 = \Delta\kappa_\gamma = -d = -d_B/\tan^2\theta_{\mathrm{W}} = 2\cos^2\theta_{\mathrm{W}}\ \Delta g_1^{\mathrm{Z}}$.

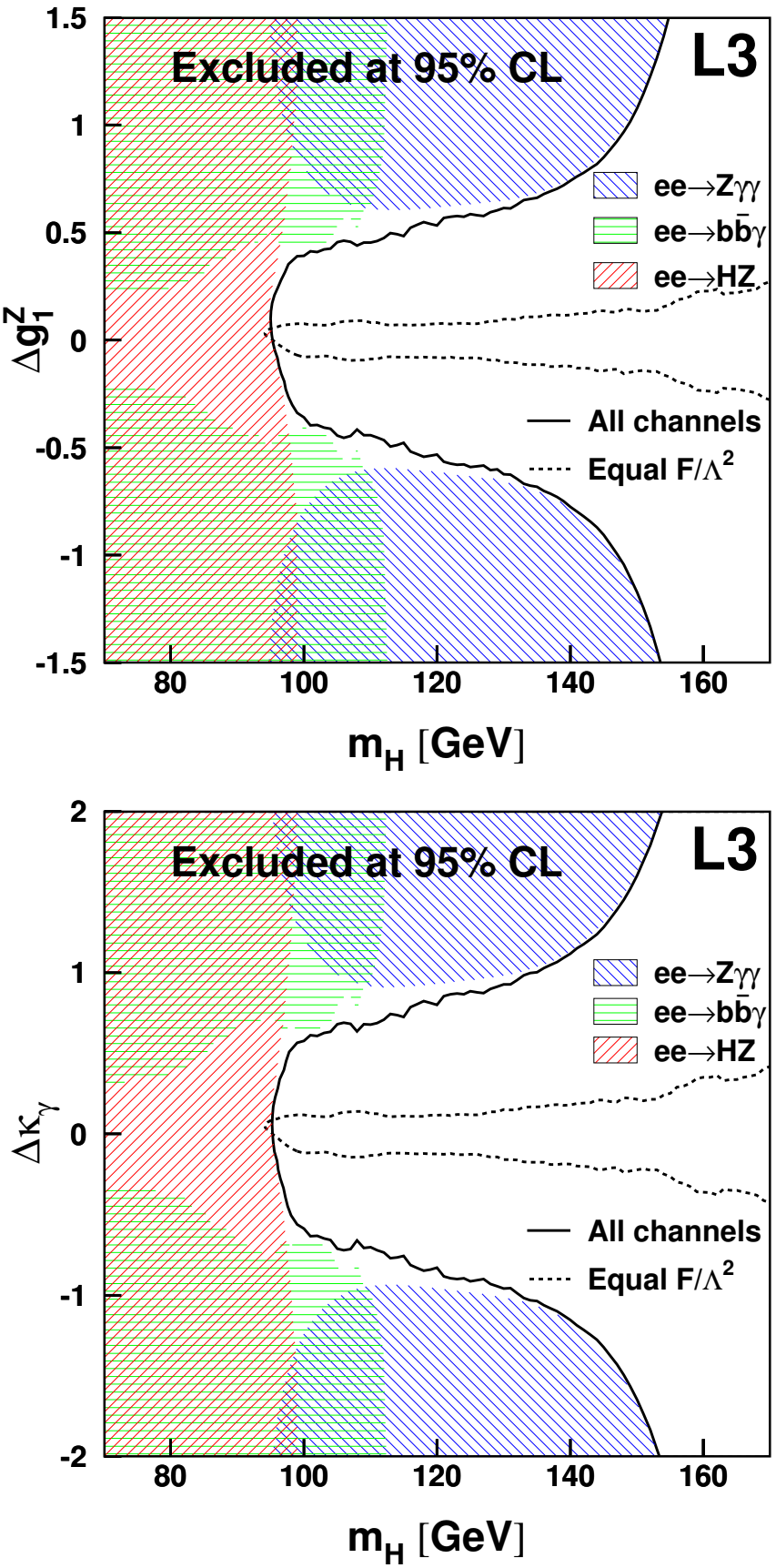

Figure 6: Excluded regions for the anomalous couplings Δg_1^Z and $\Delta\kappa_\gamma$ as a function of the Higgs mass, m_H. Limits on Δg_1^Z are obtained under the assumption $d = d_B = \Delta\kappa_\gamma = 0$, while limits on $\Delta\kappa_\gamma$ assume the relation $d = d_B = \Delta g_1^Z = 0$. The regions excluded by the most sensitive analyses: $e^+e^- \to H\gamma \to Z\gamma\gamma$, $e^+e^- \to H\gamma \to b\bar{b}\gamma$ and $e^+e^- \to HZ$ are also shown. In addition, we show the limits reached under the assumption of equal couplings at a scale of new physics Λ (dashed lines): $m_W^2\ F/\Lambda^2 = \Delta\kappa_\gamma = -d = -d_B/\tan^2\theta_W = 2\cos^2\theta_W\ \Delta g_1^Z$.

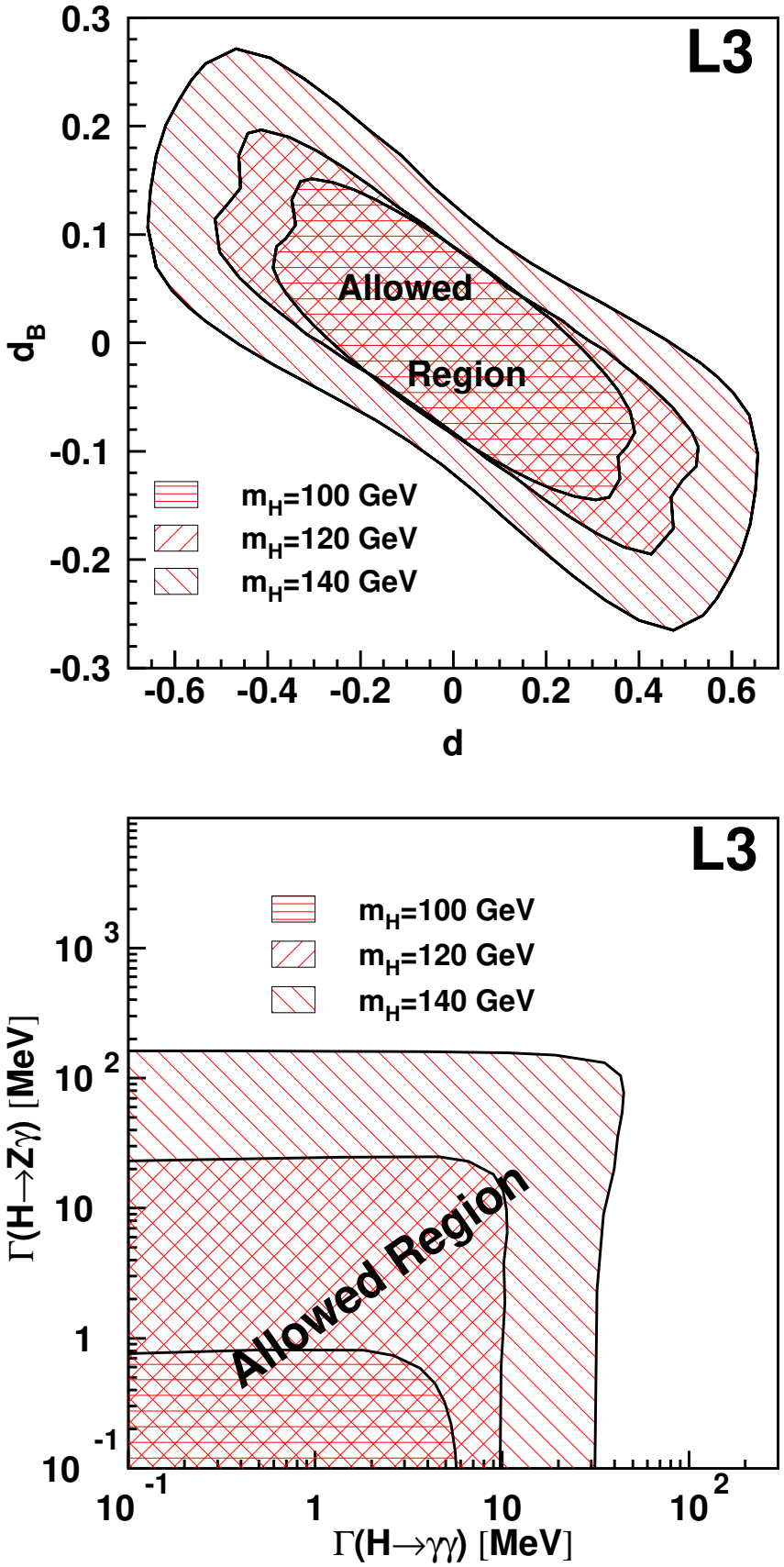

Figure 7: Allowed regions at the 95% CL in the (d, d_B) and $(\Gamma(\mathrm{H} \to \gamma\gamma), \Gamma(\mathrm{H} \to \mathrm{Z}\gamma))$ planes for different Higgs mass assumptions. All analyzed channels are used. The results are consistent with the SM expectations: $d \approx d_B \approx 0$ and $\Gamma(\mathrm{H} \to \gamma\gamma) \approx \Gamma(\mathrm{H} \to \mathrm{Z}\gamma) \approx 0$.